NASA TECHNICAL NOTE

NASA TN D-2545

NASA TN D-2545

NON-HOOKEAN, PREMACROYIELD STRESS-STRAIN BEHAVIOR OF SEVERAL IONIC SINGLE CRYSTALS

by Carl A. Stearns and Edward R. Gotsky

Lewis Research Center
Cleveland, Ohio

NATIONAL AERONAUTICS AND SPACE ADMINISTRATION • WASHINGTON, D. C. • DECEMBER 1964

NON-HOOKEAN, PREMACROYIELD STRESS-STRAIN BEHAVIOR OF SEVERAL IONIC SINGLE CRYSTALS

By Carl A. Stearns and Edward R. Gotsky

Lewis Research Center
Cleveland, Ohio

NATIONAL AERONAUTICS AND SPACE ADMINISTRATION

For sale by the Office of Technical Services, Department of Commerce,
Washington, D.C. 20230 -- Price $1.00

NON-HOOKEAN, PREMACROYIELD STRESS-STRAIN BEHAVIOR OF SEVERAL IONIC SINGLE CRYSTALS

by Carl A. Stearns and Edward R. Gotsky

Lewis Research Center

SUMMARY

The premacroyield compressive stress-strain behavior of sodium chloride, potassium bromide, lithium fluoride, potassium chloride, and magnesium oxide was studied with a refined apparatus possessing microstrain sensitivity. The stress-strain curve was found to be characterized by a general S-shape through the onset macroyielding, a lack of linearity during loading and unloading, and very low tangent moduli in the region usually considered to be elastic. The extent of the initial concave-upward region of the stress-strain curve was found to vary with specimen pretreatment, rate of testing, and prestress. Successive loading-unloading tests revealed that closed hysteresis loops result after cycling. No indication of a critical stress for overcoming Peierls-Nabarro-type barriers was observed. The experimental results are interpreted in terms of internal stresses arising from dislocation configurations.

INTRODUCTION

In a previously reported study (refs. 1 and 2) of the factors that influence the ductility and strength of several ionic single crystals, large deviations from linear elasticity were observed. While this study was not directed specifically toward investigating preyield stress-strain relations, the quality of the experiments and the magnitude of the observed deviations from Hookean behavior indicated that these results were a manifestation of some intrinsic property of the specimen under test. At that time there were no other reported indications that anything but initial linear elastic response should be observed in a stress-strain test.

More recently etch-pit studies have revealed that dislocation motion can be detected at stresses in the range heretofore considered to be Hookean. For example, Young (ref. 3) has observed dislocation motion in copper single crystals at stresses as low as 4 grams per square millimeter, and Gutmanas, et al. (ref. 4) have observed dislocation motion in sodium chloride single crystals at stresses as low as 10 grams per square millimeter.

In addition to the etch-pit evidence for the movement of dislocations at very low stresses, recent "microstrain" studies on a variety of metals (refs. 5 to 7) have revealed that nonelastic stress-strain behavior can be detected in conventional tests. The stress at which deviations from Hookean behavior are

first detected appears to be dependent on the sensitivity of the measurements (ref. 8).

Because of this new information, the details of the very early portion of the stress-strain curve for several ionic single crystals were reexamined. If dislocation mechanisms are operative here, their elucidation would certainly be important to the understanding of macroyielding and other aspects of the deformation process.

The work reported herein was concerned specifically with the details of the stress-strain curve of single-crystal sodium chloride, potassium bromide, lithium fluoride, potassium chloride, and magnesium oxide preceding macroyielding. A high-sensitivity compression test, designed to minimize prestrain effects, was developed and used (1) to establish that the previously reported shape of the stress-strain curve was indeed characteristic of the material under test and (2) to study the stress-strain curve in relation to specimen pretreatment, stress rate, strain rate, and cyclic loading-unloading.

EXPERIMENTAL

Specimen Preparation

The alkali halide crystals used in this investigation were purchased from the Harshaw Chemical Company in the form of cleaved rectangular prisms. The magnesium oxide crystals were purchased from Semi-Elements Inc. as random size cleavage blocks. Individual specimens were cleaved in this laboratory to the exact testing cross-sectional area but slightly oversize with respect to final test specimen length. To assure flat and parallel end faces, specimens were lapped by hand to the final testing length. For the lapping operation the specimen was clamped in a holder designed to facilitate the polishing of the ends flat, parallel, and perpendicular to the {100} side faces. Lapping was done dry on 2/0 to 4/0 metallographic emery polishing paper. Interferometric examination revealed that the specimen ends had a root-mean-square surface finish of 4×10^{-6} inch, were flat to within one-half the wavelength of the thallium green line, and were parallel to within 10 seconds.

Test Method

The compression apparatus developed for this study provided (1) a displacement sensitivity of 5×10^{-7} inch, (2) a load sensitivity of 5 grams, (3) uniaxial loading, (4) high-speed response, and (5) the option of constant-loading-rate or constant-deflection-rate testing. The complete apparatus is shown schematically in figure 1. This apparatus has three basic components, and because an understanding of the apparatus is essential in evaluating the experimental results, these components will be described in detail.

Loading system. - The specimen, which stands on the lapped-flat load-cell table, is loaded in compression indirectly by the movable crosshead of an Instron machine. As a step toward providing axial loading, it was found

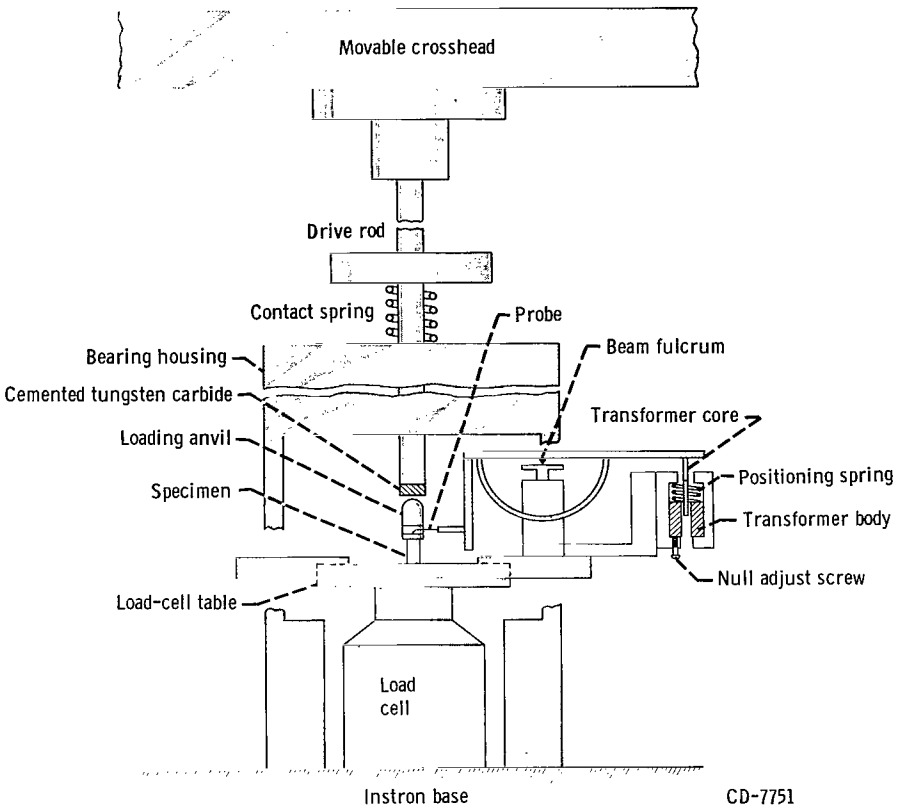

Figure 1. - Schematic drawing of compressive stress-strain apparatus.

necessary to have the movable crosshead actually push on a rod guided in a long bearing. This drive rod was a 0.75-inch-diameter, precision ground, stainless-steel shaft to which a 0.75-inch-high section of cemented tungsten carbide was brazed at the specimen end. The drive rod passed through a 7-inch-long bronze bearing housed in a massive aluminum frame. The aluminum frame was attached rigidly to the same base as the load cell. Side forces and friction in the bearing were thus not sensed by the load-weighing system. The tungsten carbide face of the drive rod was ground perpendicular to the length of the rod, and the root-mean-square surface finish was 10 microinches. The load-cell table was lapped to a root-mean-square surface finish of 4 microinches.

To obtain satisfactory uniaxial loading it was necessary to place a 30-gram stainless-steel anvil directly on the specimen and let the drive rod act on the specimen through this anvil. The anvil had a polished hemispherical top and lapped flat bottom. The root-mean-square surface finish of the flat bottom was 4 microinches, and the bottom surface was flat to one-half the wavelength of the thallium green line. In addition to providing uniaxial loading, the anvil served a definite function in the deflection-measuring system (described in the section Displacement-measuring system).

As mentioned previously, two modes of testing were available with this loading system, namely, constant loading rate and constant deflection rate. By maintaining the drive rod in direct contact with the movable crosshead,

constant deflection rates were produced; when a rubber cylinder of low stiffness was inserted between the drive rod and crosshead, constant loading rates were produced. Contact between the crosshead and the drive rod (with or without the rubber cylinder) was maintained by holding a spring in compression between a collar, attached to the drive rod, and the bearing housing. Rates were adjusted by changing crosshead speed or the compliance of the rubber cylinder or both. Rates were determined from independently recorded load-time or deflection-time curves.

Load-weighing system. - The basic element of this system was an Instron type CD (1000-lb max. capacity) load cell. This high-capacity cell was selected to keep the entire system as hard as possible for the constant-deflection-rate mode of testing. The deflection coefficient of the system was measured and found to be 2×10^{-6} inch per pound.

The load cell was operated with an Instron bridge amplifier. The output of the phase-sensitive detector associated with the amplifier was fed through a high-cutoff filter directly to the y-axis of an 11- by 17-inch x-y recorder. The load-weighing system was calibrated by dead-weight loading, and the sensitivity was determined to be 100 grams per inch of chart on the x-y recorder.

Displacement-measuring system. - Specimen deflection was measured with a linear variable differential transformer (LVDT) and balanced-beam arrangement as shown in figure 1. The beam fulcrum and the LVDT body were mounted on the load-cell table so that any deflection in the load-weighing system was not detected by the displacement measuring system. At opposite ends of the beam were attached a probe, which followed the specimen, and the LVDT core, which was free to move with respect to the LVDT body. Only a slight magnification was offered by the ratio of the beam-arm lengths, the ratio of arm lengths being 1.28. The beam was unbalanced in the probe direction by placing a 2-gram weight at the end of the beam. In practice, the probe rested at the bottom of a 0.125-inch-high by 0.065-inch-wide slot through the previously described loading anvil. The 2-gram beam unbalance thus provided that the LVDT core would follow the specimen deflection.

The LVDT used had a basic sensitivity of 40 microvolts output per microinch of displacement when driven by 6 volts root mean square at 1.5 kilocycles. To realize this maximum sensitivity from the LVDT and to make the device linear through the null position, noise effects had to be eliminated completely. This was readily accomplished by using a lock-in amplifier, which is a narrow-band, coherent detector that includes a high-Q continuously tunable selective amplifier, a phase-sensitive detector, a direct-current amplifier, a phase-control, signal-modulating oscillator, and a recorder-drive circuitry.

The displacement measuring system was calibrated by allowing the beam probe to follow the Instron crosshead directly and by recording the motion measured by the LVDT against time. Crosshead displacement rates were determined with a dial indicator sensitive to 0.0001 inch and a stop watch. The calibration displacement-time curves were linear to the extent that for a total deflection of 0.00125 inch no deviations from linearity greater than 2.5×10^{-6} inch could be detected.

As pointed out previously, a 30-gram loading anvil and a 2-gram beam unbalance were essential parts of the test arrangement. The 32-gram load was in all cases imposed on the specimen and thus represented an initial load or stress bias. In all the data presented herein the zero applied load or stress axis refers to the stress applied in addition to the stress bias noted with each curve.

Two types of dynamic mechanical devices were used to condition some specimens. One of these was a Fitzgerald-type dynamic shear transducer (ref. 9) in which specimens were sheared while under a static compressive clamping stress. The second device consisted of a sandwich construction lead zirconate-titanate (PZT) transducer on which the specimen stood upright. This consisted of two 0.5-inch-diameter by 0.25-inch-high PZT disks with silvered electrodes on the end faces cemented together. The outside electrodes were paralleled to ground, and the center electrode of the sandwich was positive. The transducer was energized by 40 volts root mean square derived from a variable-frequency oscillator. In both dynamic treatments the maximum displacement amplitude was 1×10^{-6} inch.

RESULTS

Stress-Strain Curve

A typical load-deflection curve into the macroyield region is shown in figure 2 for as-cleaved sodium chloride. This curve was generated in a constant-strain-rate compression test. For comparison purposes the Hooke's law line for this specimen, calculated from elastic constant data for sodium chloride (ref. 10), is also shown. An as-recorded load-deflection trace is presented to show the quality of the recorded data. Since all the measured deflection is that of the specimen under test and since the measured load is that applied to the specimen, no corrections are required to compute the stress-strain curve. The load-deflection curve has the same shape as the stress-strain curve and in fact becomes the stress-strain curve when the axes are scaled by the specimen's cross-sectional area and initial length, respectively.

The curve shown in figure 2 is seen to be characterized by (1) a general S-shape through macroyielding (an initial concave-upward portion, termed the foot, followed by a concave downward portion starting at the inflection point), (2) a lack of linearity during loading, (3) very low tangent moduli in the region generally considered to be elastic, and (4) a nonlinear unloading curve. While the magnitude of the details of the stress-strain curve (such as the foot length, which is approximately the ratio of strain to inflection point) varied considerably from specimen to specimen for presumably identical crystals prepared identically, these four features were always obvious for specimens tested at either constant deflection rate or constant loading rate. Furthermore, curves of the same general shape were observed for single-crystal potassium chloride, lithium fluoride, potassium bromide, and magnesium oxide.

The shape of the stress-strain curve herein observed for these ionic crystals is unconventional up to the inflection point in that the initial curvature

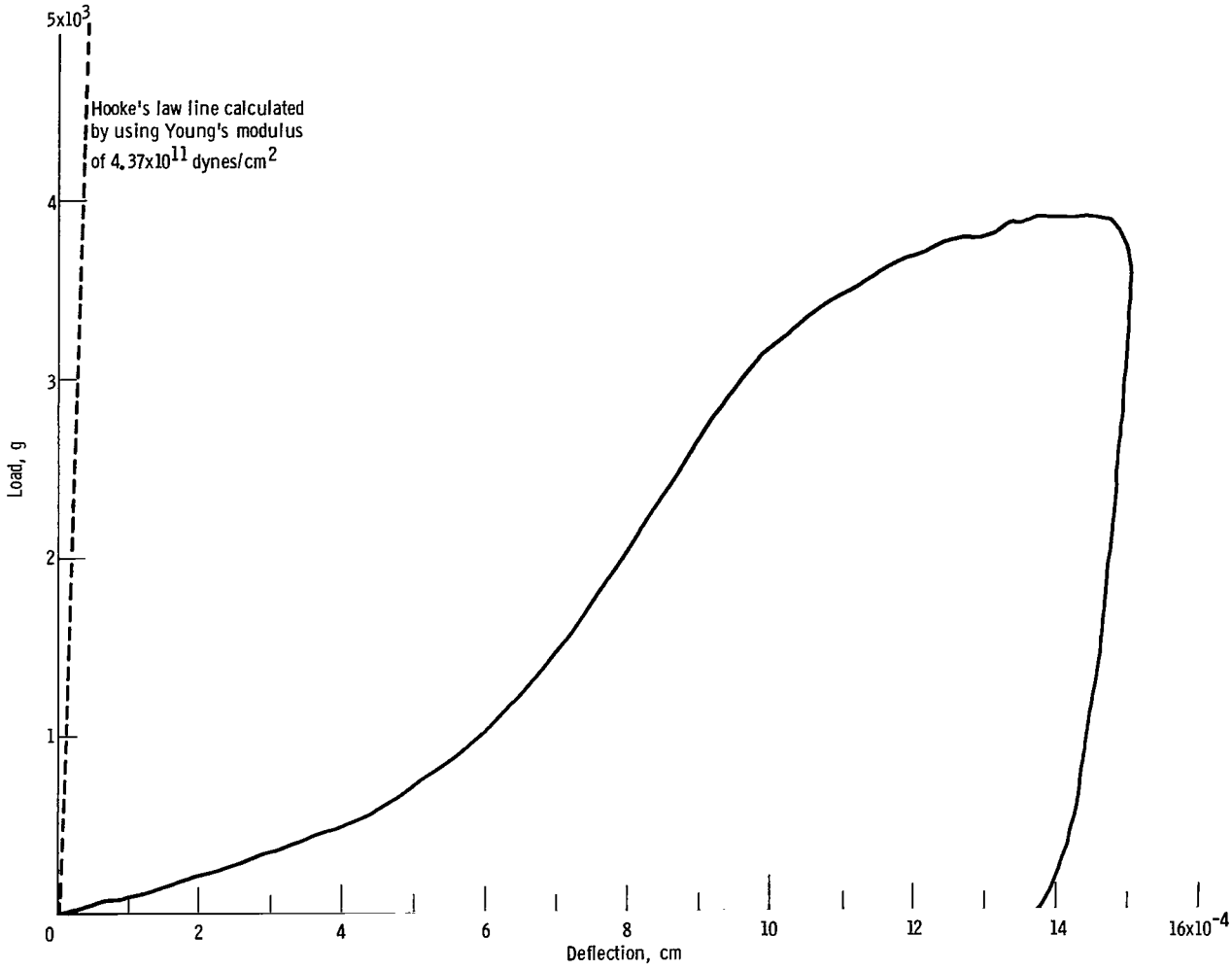

Figure 2. - As-recorded, load-deflection trace for cleaved sodium chloride single crystal tested in compression. Specimen area, 49.437 square millimeters; length, 18.39 millimeters; strain rate, 1.15×10^{-4} per second; stress bias, 0.65 gram per square millimeter.

is concave upward. Beyond the inflection point the shape of the curve is qualitatively similar to that observed by other investigators (refs. 11 to 13), and the stress range for macroyielding is in agreement with the values reported in the literature (ref. 14).

Although all test conditions (axiality, system response, specimen geometry, surface finish of specimen ends, etc.) were considered to be excellent, it was recognized that the initial curvature observed could conceivably be due to factors inherent in the test rather than in the specimen. Specific tests were performed to ascertain whether this shape was characteristic of the specimen or an artifact of the test. While all these tests indicated that the shape was inherent to the specimen, the best proof was provided by the following experiment.

A specimen was subjected to three loading-unloading cycles to a maximum stress below the inflection point stress. These three cycles are shown in figure 3. From figure 3 it is obvious that a residual strain is associated

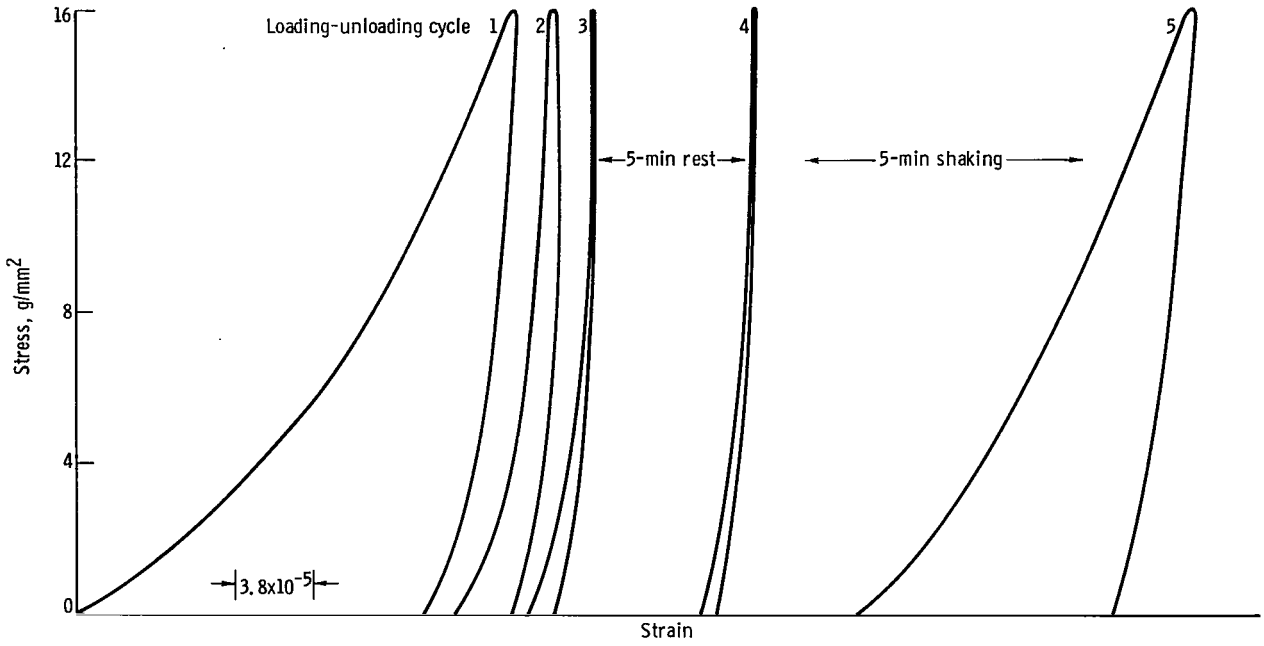

Figure 3. - Initial portion of compressive stress-strain curve showing effects of repeated loading and unloading and audiofrequency shaking. Specimen length, 18.5 millimeters; strain rate, 1.20×10^{-4} per second.

with each cycle. This residual strain decreases with each successive cycle. After many successive cycles, the residual strain would become zero (described in detail in the section Cyclic Loading and Unloading). After cycle 3 the specimen was removed from the compression apparatus and placed gently on the PZT transducer. The transducer was not energized and the specimen was allowed to remain on the transducer for 5 minutes. Next the specimen was returned to the compression apparatus and a fourth loading-unloading cycle was performed (cycle 4 in fig. 3). From 4 it is seen that the residual strain decreased as expected, and the 5-minute rest on the transducer plus the transfer time had virtually no effect on cycle 3. Again the specimen was removed from the compression apparatus and placed on the PZT transducer. This time the transducer was energized by 40 volts root mean square. The frequency of the energizing voltage was varied from 100 to 10^4 cps in a random scanning manner. After 5 minutes of shaking by the transducer (max. amplitude, 1×10^{-6} in.), the specimen was returned to the compression apparatus, and the fifth cycle (cycle 5 in fig. 3) was performed. Inspection of figure 3 reveals that the residual strain associated with 5 increased compared with 4 or 3. This increase in residual strain is taken to show that the foot has been at least partially regenerated.

Similar tests were performed with the Fitzgerald dynamic shear apparatus used for the shaking instead of the PZT transducer. These tests also showed that the foot could be regenerated.

The increase in residual strain, associated with a loading-unloading cycle, after shaking can only be attributed to internal changes in the specimen caused by the shaking. The experiments were performed in a manner that eliminated

possible time effects, and the amplitude of the shaking was too small to cause external alterations to the specimen, such as geometry changes, etc. These results, together with the fact that the stress-strain curves for specimens prepared in identical fashion vary in detail, lead to the conclusion that the observed curvature of the stress-strain curve is a manifestation of the intrinsic structure of the specimen under test and not an artifact of the test. Additional factors that further substantiate this conclusion will be pointed out as other experimental results are presented.

Effects of Specimen Pretreatments

Specimens annealed for 10 hours at 100° C below their melting point and specimens irradiated with 2-Mev electrons or 70 to 250-kilovolt X-rays showed the same general shape stress-strain curve noted previously. For annealed sodium chloride the general stress level for macroyielding was slightly lower than that observed for as-cleaved specimens. Electron irradiation raised the general stress level for the macroyielding of sodium chloride by a factor of about 40 above that for as-cleaved specimens, and X-ray irradiation raised it by a factor of about 10. (Exact values depend on dose, but are not important for considerations presented herein.)

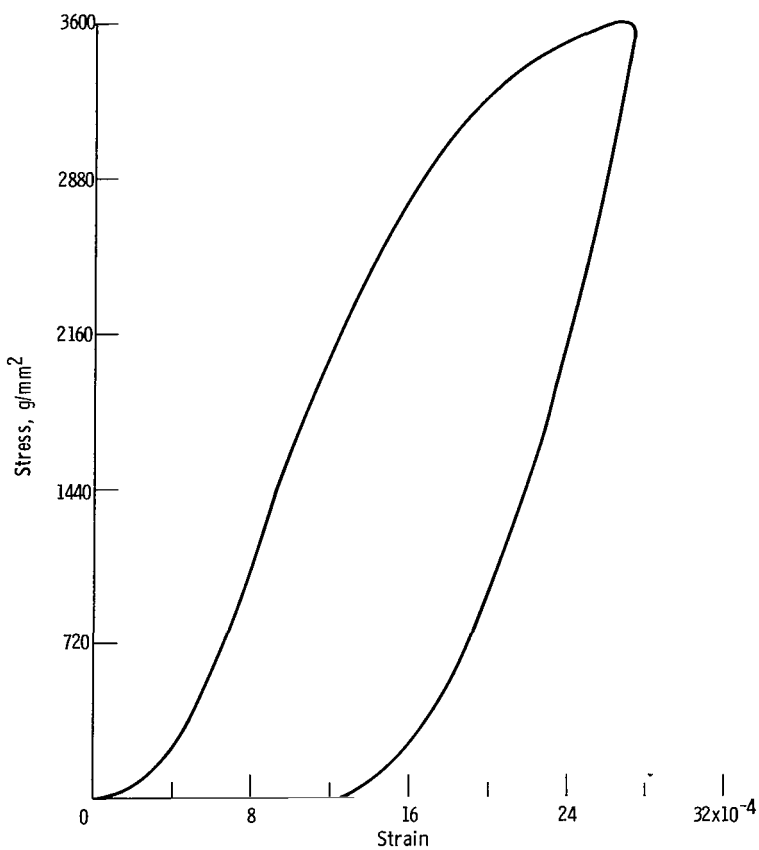

Figure 4. - Compressive stress-strain curve for electron-irradiated sodium chloride. Irradiation for 1 hour by 2-Mev 10 microampere beam; stress bias, 0.60 gram per square millimeter; strain rate, 2.05x10^{-4} per second.

In addition to these changes in the macroyield level, the various pretreatments effected changes in the foot length. Annealing reduced the foot length slightly, and the irradiations increased the foot length as compared with as-cleaved specimens.

The stress-strain curve for an electron-irradiated sodium chloride specimen is shown in figure 4. Irradiation time was 15 minutes on a side in a 2-Mev 10 microampere beam; the irradiation was done in air. From figure 4 it can be seen that the four features noted previously are still present even though the scale required to show the curve through macroyielding is greatly compressed as compared with figure 2. On this scale portions of the curve appear almost linear, but when the curves for

similarly treated specimens were recorded with high sensitivity, the lack of linearity was more apparent.

When the irradiated specimen of figure 4 was repeatedly loaded and unloaded (max. stress of 3600 g/mm^2) nine times, the ninth cycle had no residual strain associated with it, and the maximum tangent modulus was 4.29×10^{11} dynes per square centimeter. This value is within about 1 percent of the value derived from elastic constant calculations and clearly shows that the experimental arrangement is indeed capable of measuring high modulus values.

Testing Rate and Size Effects

All the results presented heretofore hold for specimens tested in constant-strain-rate or constant-stress-rate compression. Definite rate dependencies, however, were observed, especially with regard to the foot of the stress-strain curve. In figures 5(a) and (b) are plotted the initial portions of the stress-strain curves for sodium chloride; these curves were generated in a constant-stress-rate compression test, and individual stress rates were determined from independently recorded load-time curves. To minimize variations from one crystal to another, the two specimens of figure 5(a) and the two specimens of figure 5(b) were each cleaved from the same parent prism. The cross-sectional dimensions were cleaved first; then the prism length was bisected. From figure 5 it can be seen that, the slower the stress rate, the larger the foot. Curves generated at rates intermediate to those shown in figure 5 showed the same general trend.

Typical results of constant-strain-rate tests are presented in figure 5(c) for sodium chloride. Again all the specimens represented by the curves in this figure were cleaved from the same parent prism. For the range of rates examined, the foot increased with decreasing strain rate.

A comparison of the curves shown in figures 5(a) and (b) reveals that an apparent size effect exists with regard to the foot of the stress-strain curve. When this size effect is investigated, the strain-rate and the stress-rate effects complicate matters because during any test only one of these rates can be held constant. For example, samples of equal cross section tested at a constant crosshead speed with a single rubber cylinder yielded a constant loading or stress rate, but obviously the strain rate changed with sample length. Thus foot variations observed with changes in sample length might be due to the change in strain rate or the change in length or both. For this reason all size effects observed are referred to as apparent size effects.

Apparent size effects have been observed in both constant-strain-rate and constant-stress-rate tests. In figure 5(d) are plotted stress-strain curves generated in a constant-strain-rate test. For the three curves shown the strain rate was approximately constant, but the specimen length was varied by a factor of nearly 6. The three specimens represented in this figure were cleaved from the same initial stock. The results shown in figure 5(d) indicate that shorter specimens produce a larger foot on the stress-strain curve.

Rate and size effects in lithium fluoride, potassium bromide, potassium chloride, and magnesium oxide have only been examined in a very preliminary fashion, but indications are that the same general trends are followed as in sodium chloride. Detailed studies of these effects in sodium chloride as well as in potassium chloride, potassium bromide, and magnesium oxide are to be the object of further investigation.

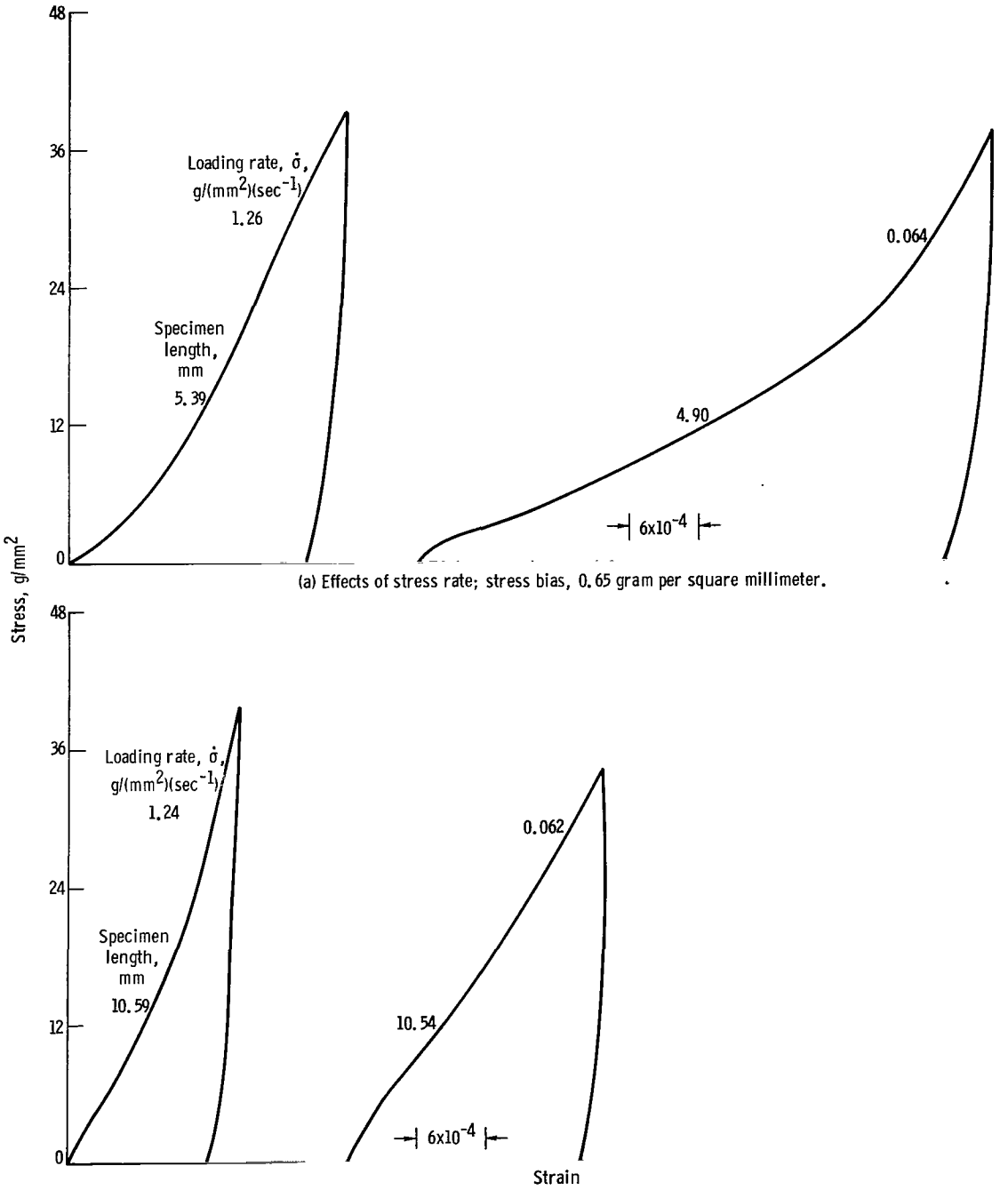

(a) Effects of stress rate; stress bias, 0.65 gram per square millimeter.

(b) Effects of stress rate; stress bias, 0.64 gram per square millimeter.

Figure 5. - Initial portion of constant-stress-rate compressive-stress-strain curves for cleaved sodium chloride specimens.

Cyclic Loading and Unloading

Repeated loading-unloading tests were performed on the five ionic single crystals studied in this investigation. These tests are referred to as cyclic, but the exact nature of the cycle is such that the specimen is only subjected to an applied unidirectional force. The specimen is compressed, but not pulled back. For a constant-strain-rate test, compressive loading proceeds by way of the constant applied strain rate, and unloading takes place when the drive rod is backed off the specimen at the same constant rate used during loading. For the constant-stress-rate test, loading and unloading proceed at a constant application and removal of load.

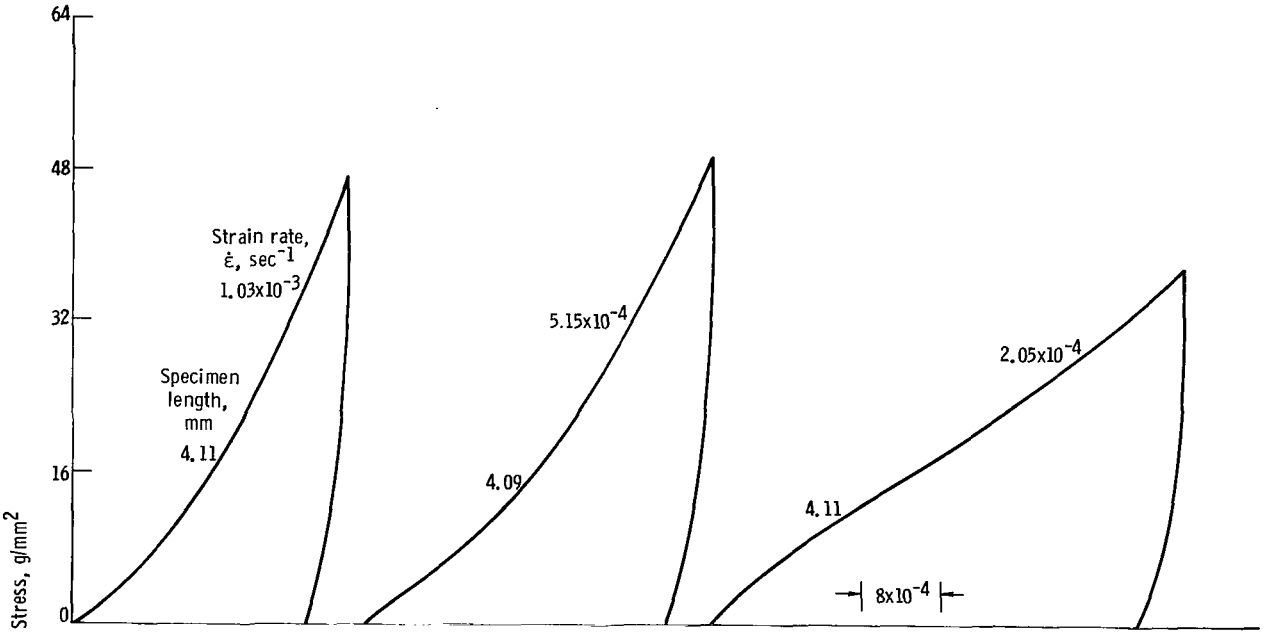

(c) Effects of strain rate; stress bias, 0.65 gram per square millimeter.

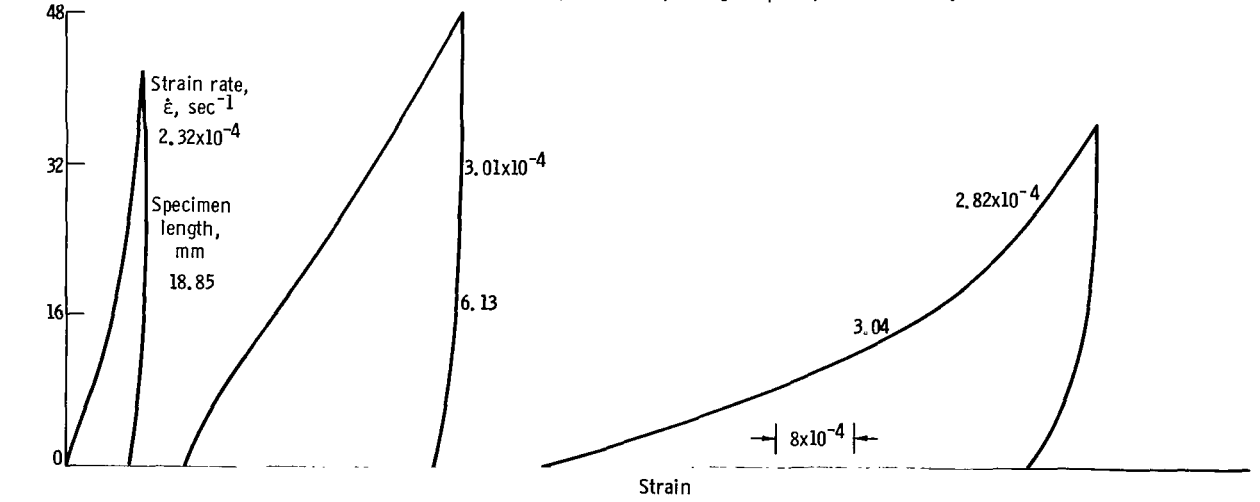

(d) Effects of specimen size; stress bias, 0.65 gram per square millimeter.

Figure 5. - Concluded. Initial portion of constant-stress-rate compressive-stress-strain curves for cleaved sodium chloride specimens.

When a cycle (load and unload) was performed for the first time, an open hysteresis loop resulted (i.e., there was residual strain associated with the cycle). Upon reloading, the curve almost followed the first cycle unloading curve. If in the second cycle the maximum stress of the first cycle was not exceeded, the second-cycle loop was not as open as the first; that is, the residual strain was reduced. With each successive cycle to loads equal to or less than the first-cycle maximum, the loops closed further until finally a completely closed loop was formed. Closed loops may be traversed any number of times in a remarkably reproducible manner. Once a closed loop was formed, it could be made to open in the next cycle if the maximum stress of the preceeding cycles was exceeded. Again more cycling to below the new maximum stress produced a closed loop. An example of cyclic tests showing this behavior is presented for magnesium oxide in figure 6 where a recorded load-deflection trace is shown.

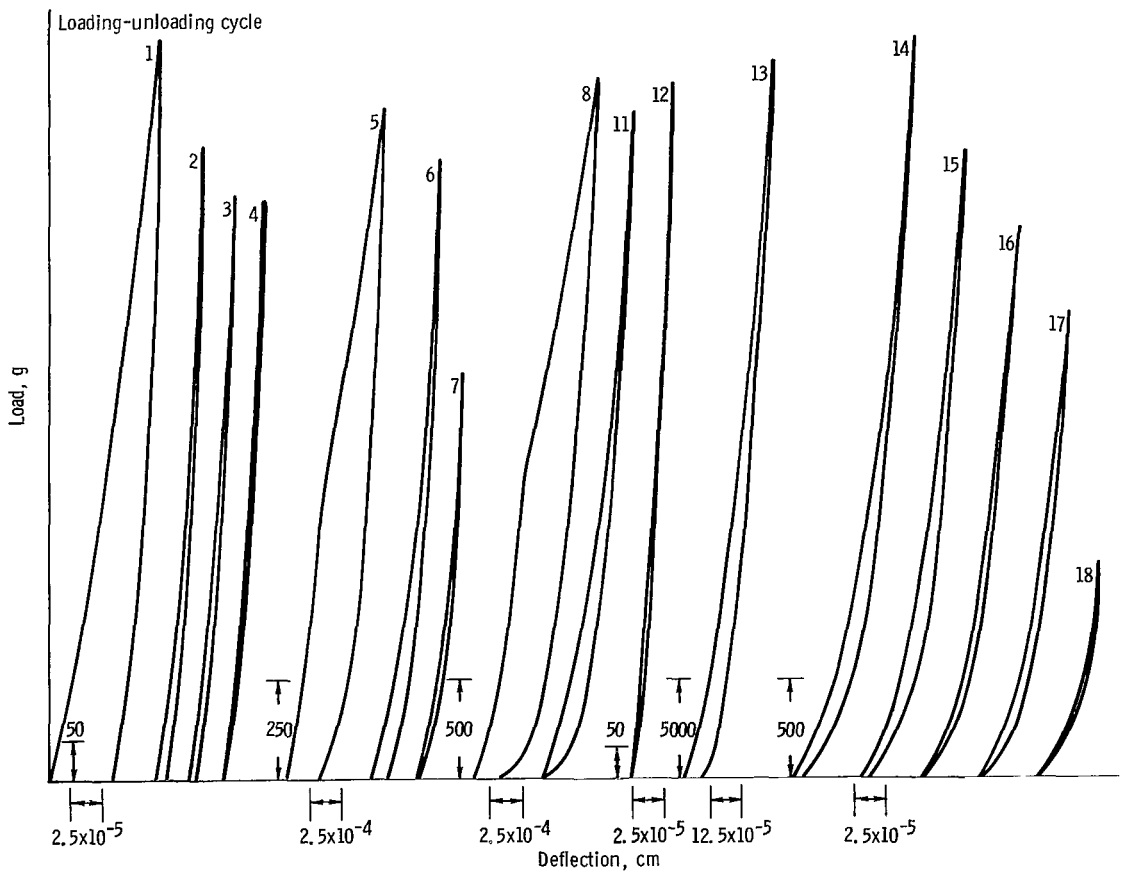

Figure 6. - Successive constant-strain-rate loading-unloading, load-deflection curves for cleaved magnesium oxide. Specimen area, 33.62 square millimeters; length, 18.49 millimeters; strain rate, 1.15×10^{-4} per second; stress bias, 0.95 gram per square millimeter.

Generally, many cycles were required to form closed loops if the maximum stress was below the macroyield stress, but if the maximum stress was well into the macroyield region, only a few cycles were needed to produce closed loops.

Results representative of this behavior are shown in figure 7 for potassium bromide.

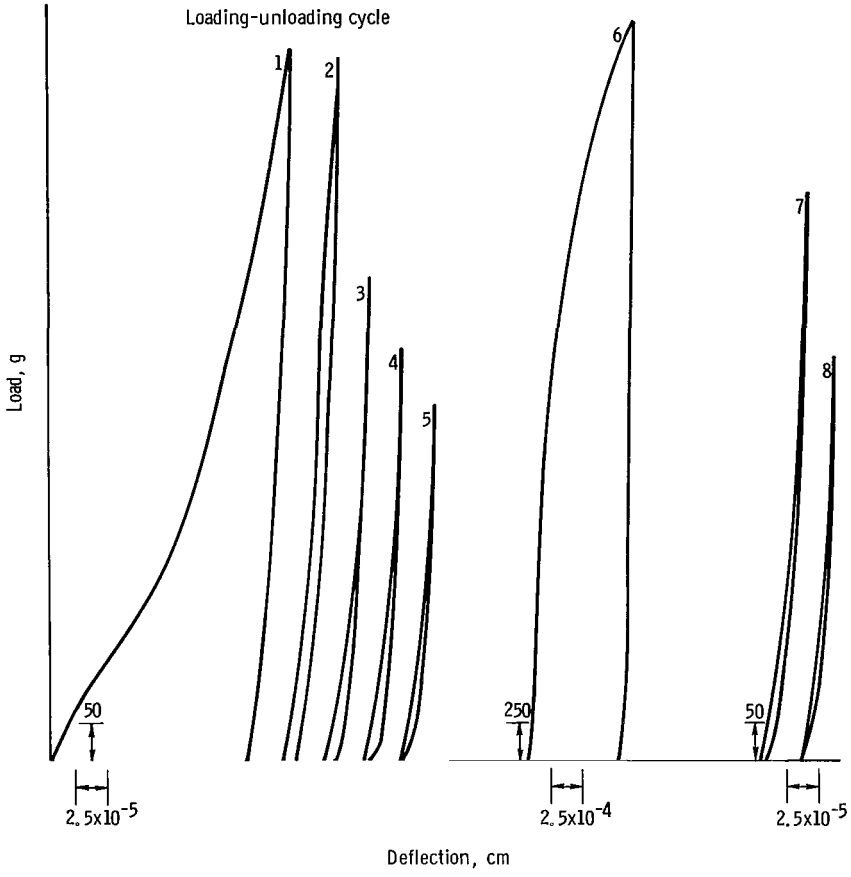

Figure 7. - Successive constant-strain-rate loading-unloading, load-deflection curves for annealed potassium bromide. Specimen area, 30.09 square millimeters; length, 18.42 millimeters; strain rate, 1.16×10^{-4} per second; stress bias, 1.07 grams per square millimeter.

Relative time was found to be an important factor when observing hysteresis loops. Open loops were often seen to tend toward closing at zero applied stress; for very open loops (first few cycles) times of the order of hours were required for any closing, but for nearly closed loops (those formed after many cycles) closing was often observed in seconds, and usually the closing was not continuous but stepwise. These observations on sodium chloride are the same as those reported by Roberts and Brown (ref. 5) for zinc. A further aspect of this effect of time was observed when specimens were allowed to age in place at zero applied stress after a few cycles to stresses below the inflection-point stress. The loop formed after the aging period was found to be more open than the last loop formed before aging; if sufficient aging time was allowed to elapse (>24 hr), the first cycle was almost completely reproduced.

Another effect of testing rate was seen when successive loops were generated at different rates. A typical group of results is shown in figure 8. Ten loading-unloading cycles (not shown) to a maximum load of 2400 grams were performed in a constant-stress-rate test. The crosshead speed for the first 10 cycles was 0.5 inch per minute, which produced a loading rate of approximately 6 grams per square millimeter per second. Cycle 11 was executed at this same crosshead speed; the maximum load was 500 grams. Immediately thereafter, the crosshead speed was reduced to 0.05 inch per minute, and cycle 12 was performed. After cycle 12, the crosshead speed was reduced still another factor of 10 to 0.005 inch per minute, and cycle 13 was generated. From figure 8 it is obvious that the loop became more open as the rate was reduced; this is

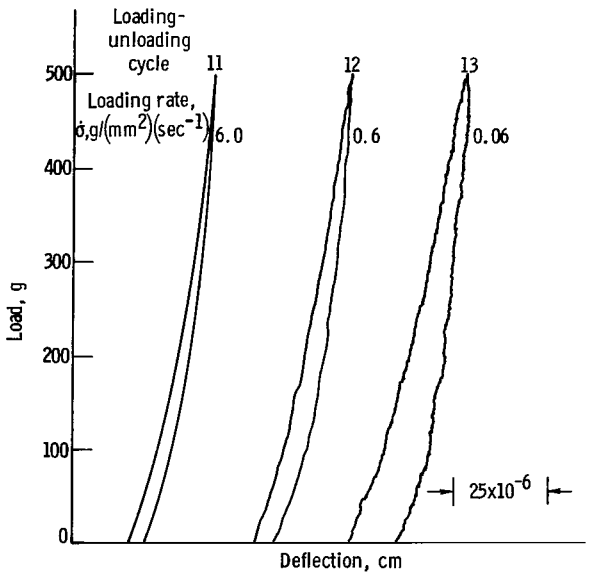

Figure 8. - Successive loading-unloading, load-deflection curves for cleaved sodium chloride. Irradiated for 10 minutes by 2-Mev 15 microampere beam; specimen area, 49.558 square millimeters; length, 18.78 millimeters.

opposite to what was observed when all three loops were generated at the same rate. Also to be noted in figure 8 is the fact that the slowly traversed loop is considerably serrated; whereas, the loop generated at the high rate is not.

In the course of this investigation it was consistently observed that, at the slower rate of testing (whether constant strain rate or constant stress rate), the loops were larger, more cycles were required to produce closed loops, and the loading and unloading curves were more irregular.

The effects of performing successive cycles to increasing maximum stress are shown in figure 9. From this figure it can be seen that, each time a successive cycle is generated to a higher load than the preceeding cycle, the slope of the new cycle loading curve becomes smaller after the maximum load of the preceeding cycle is exceeded. For brevity some of the cycles have been omitted.

It is to be noted that this change to a lower slope takes place at all stress ranges, even before the inflection point and macroyield region. This effect is identical to that generally observed in the macroyield or gross-plastic-deformation part of the stress-strain curve of a wide variety of other materials. In many of the tests performed, similar changes in slope were noted

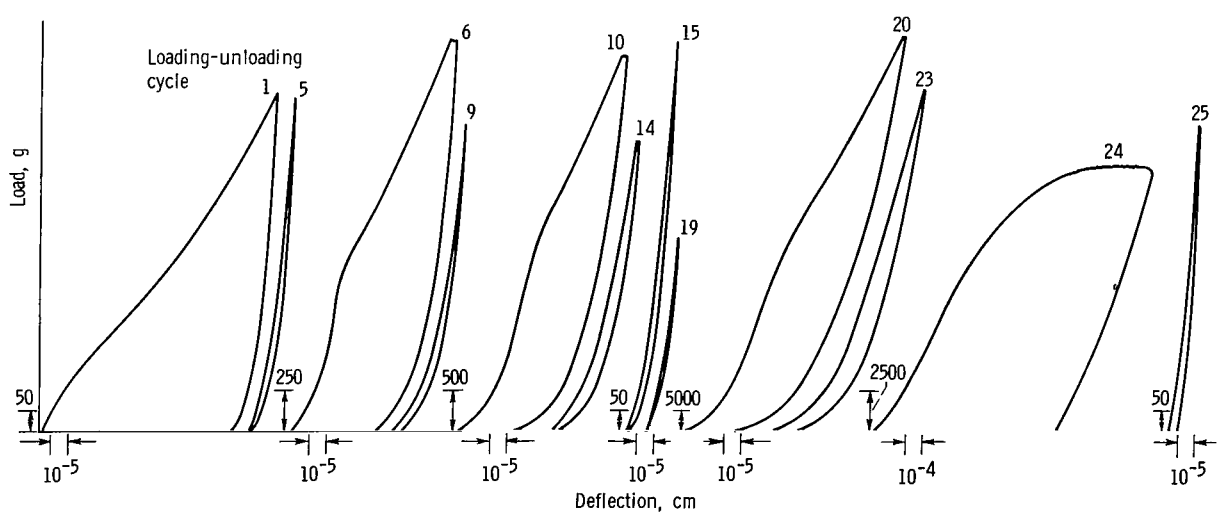

Figure 9. - Constant-strain-rate loading-unloading, load-deflection curves for electron-irradiated sodium chloride. Irradiation, 2-Mev electrons; specimen area, 50.45 square millimeters; length, 18.49 millimeters; strain rate, 1.15x10^{-4} per second.

in the initial loading curve at very low stresses (e.g., figs. 5(a) to (c)). These changes in slope of the initial loading curve are believed to be the result of small strains introduced by handling prior to testing. The very low initial modulus here observed makes it reasonable to expect that such strains could occasionally be introduced even with careful handling.

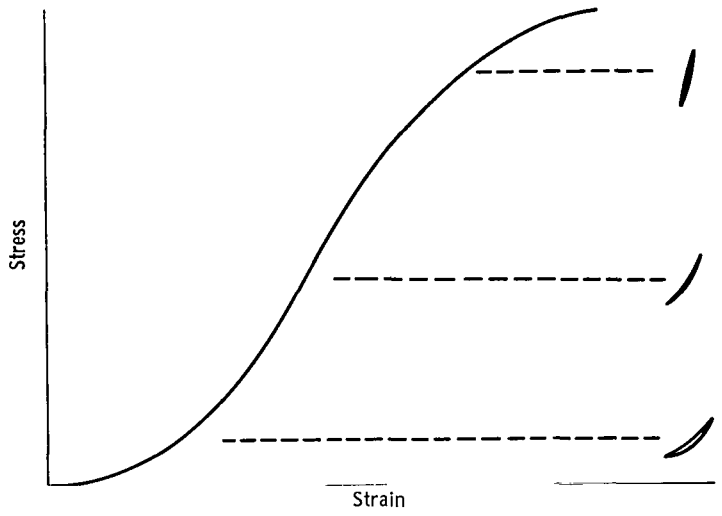

Figure 10. - Schematic compressive stress-strain curve showing shape of loop obtained at various bias stress levels.

Localized cyclic loading and unloading about various compressive stress levels (i.e., about a bias stress) revealed that the shape of the loop transversed depends on the stress level about which the cycling is performed (shown schematically in fig. 10). At low stress levels the loop is crescent shaped and the general slope of the loop is small. At stress levels above the inflection point the loop takes on the appearance of more conventional hysteresis loops, and the slope is increased (i.e., the loop stands more erect).

DISCUSSION

The most striking feature exhibited by the experimental results is the initial low-slope, concave-upward region of the stress-strain curve. All of the experimental results establish that the foot is a manifestation of a real deformation mode of the material under test. The effects of dynamic shaking, pretreatments, testing rate, and cyclic loading-unloading cannot be adequately explained in terms of an artifact of the testing procedure.

At the present time a specific detailed model to explain all the experimental results is not available; however, when the results are interpreted in terms of a simple physical scheme involving dislocation, the shape of the stress-strain curve appears to be compatible with existing dislocation concepts. Since the results show no indication of a critical stress for overcoming barriers, such as the Peierls-Nabarro type, the scheme must first account for dislocation motion at near-zero applied stress.

There is ample evidence in the literature to show that all materials contain complex dislocation arrays. With the large dilatation characteristic of dislocations and the normal densities of dislocations observed by etch-pit methods, the presence of a large internal stress field is to be expected. The exact nature of the stress field for any specimen will be determined by the configuration of the dislocation array. It is not unreasonable to assume that the configuration will be such that the internal stresses will, under the action of an applied external stress, enhance the movement of some dislocations

and oppose the motion of others. The specimen will thus have dislocations available for motion at low applied stresses. The strain response of the specimen will be governed by the number of dislocations that can move at the lowest velocity consistent with the applied stress and with the ever changing internal stress distribution.

On the basis of this scheme, the relatively large strains at low applied stress are the result of dislocation motion caused by the local resultants of the applied and internal stresses. At low stresses, dislocations move at low velocities (ref. 4). As the deformation proceeds, the stress-field interactions are altered such that further dislocation motion becomes more difficult to attain. As more dislocations lose their mobility, the applied stress needed to maintain the imposed deformation rate rises, the stress-strain curve increases in slope, and the dislocation velocity increases. Eventually the applied stress reaches a sufficiently high level to allow another deformation mechanism to predominate. This stress level is near the inflection-point stress. The mechanism operating at these higher stresses may involve the generation of more dislocations or the attainment of higher mobilities or both. In any event, the product of the number and velocity of the dislocations in the specimen starts to increase, and hence, the slope of the stress-strain curve begins to decline.

The nonlinear unloading curve and residual strain associated with the stress-strain curve can also be interpreted on the basis of the proposed scheme. The residual strain is attributed to the change in configuration of the dislocation array while the nonlinear, nonelastic unloading curve is believed to be primarily a consequence of the reverse motion of dislocations that were forced into barriers and high-energy configurations during the loading cycle. Subsequent loading cycles that do not exceed the maximum applied stress of the first cycle display the effects of additional configurational changes. The unloading curve measures the recovered strain caused by the back forces. When the former contributes strains less than 5×10^{-7} (the strain resolution limit of these experiments), the loops appear closed. The shape of a closed loop measures only the reversible motion of dislocations into barriers. The concave-upward shape of the closed loops displays the increase in stiffness that a dislocation experiences as it moves into barriers.

When the maximum applied stress of previous cycles is exceeded in a subsequent cycle, the stress-strain curve undergoes a radical change in slope. This change is due to the additional configuration changes, which are now possible under the higher applied stress. Thus, additional residual strain is obtained on unloading.

Specimen pretreatments that produce changes in the dislocation structure would, according to this proposed scheme, be expected to affect the foot of the stress-strain curve. Certainly, such treatments as annealing, prior straining, and irradiation alter the dislocation structure; however, the way these changes are effected, as well as the type of changes in dislocation structure, is largely a matter of speculation beyond the scope of this report.

SUMMARY OF RESULTS

From a study of the premacroyield compressive stress-strain behavior of sodium chloride, potassium bromide, lithium fluoride, potassium chloride, and magnesium oxide, the following results were obtained:

1. The compressive stress-strain curve is characterized by a general S-shape through macroyielding, a lack of linearity during loading and unloading, and very low tangent moduli in the region generally considered to be elastic.

2. Pretreatments such as annealing and irradiation do not alter the general shape of the stress-strain curve but do alter individual details such as the length of the initial concave-upward portion (or foot) and the macroyield stress level. Annealing reduces the foot and macroyield stress level; irradiation increases both the foot length and the macroyield stress level.

3. Rate of testing is important to the magnitude of the details of the stress-strain curve. Low rates of testing result in a large foot and very open hysteresis loops. High rates of testing result in a reduced foot and less open hysteresis loops.

4. The extent of the foot is a function of prestrain. Cyclic prestraining and prestrains introduced during handling result in a reduced foot.

5. The nature of cyclic loading-unloading hysteresis loops depends on time. Loops close with time at zero stress, and the enclosed area of the loop depends on the time of traversal. The longer the traversal time, the larger the enclosed area.

6. The shape of a loop formed by cycling about a bias-stress level depends on the magnitude of the bias stress. At low stresses the loop is crescent shaped, and at high stress the loop is erect and conventional in appearance.

Lewis Research Center
National Aeronautics and Space Administration
Cleveland, Ohio, September 14, 1964

REFERENCES

1. Stearns, C. A., Pack, A. E., and Lad, R. A.: Factors Affecting the Ductility and Strength of NaCl Single Crystals Tested in Flexure. Jour. Appl. Phys., vol. 31, no. 2, Feb. 1960, pp. 231-234.

2. Stearns, Carl A., Pack, Anne E., and Lad, Robert A.: Ductile Ceramics. I - Factors Affecting the Plasticity of Sodium Chloride, Lithium Fluoride, and Magnesium Oxide Single Crystals. NASA TN D-75, 1959.

3. Young, F. W., Jr.: Elastic-Plastic Transition in Copper Crystals as Determined by an Etch-Pit Technique. Jour. Appl. Phys., vol. 32, no. 10, Oct. 1961, pp. 1815-1820.

4. Gutmanas, E. Yu., Nadgornyi, E. M., and Stepanov, A. V.: Dislocation Movement in Sodium Chloride Crystals. Soviet Phys.-Solid State, vol. 5, no. 4, Oct. 1963, pp. 743-747.

5. Roberts, J. M., and Brown, N.: Microstrain in Zinc Single Crystals. Trans. Met. Soc. AIME, vol. 218, June 1960, pp. 454-463.

6. Brown, N., and Lukens, K. F., Jr.: Microstrain in Polycrystalline Metals. Acta Met., vol. 9, no. 2, Feb. 1961, pp. 106-111.

7. Washburn, J., Parker, E. R., and Tinder, R. F.: Deformation Processes in Materials. Final Rep., Issue 22, Ser. 27, Univ. Calif., Aug. 1962.

8. Tinder, R. F.: Initial Plastic Behavior of Zinc. Paper Presented at Microstrain Symposium, Met. Soc. AIME, N.Y. (N.Y.), Feb. 16-20, 1964.

9. Fitzgerald, E. R., and Ferry, J. D.: Method for Determining the Dynamic Behavior of Gels and Solids at Audio-Frequencies; Comparison of Mechanical and Electrical Properties. Jour. Colloid Sci., vol. 8, 1953, pp. 1-34.

10. Huntington, H. B.: Elastic Constants of Crystals. Solid State Phys., Vol. 7, F. Seitz and D. Turnbull, eds., Academic Press, Inc., 1958.

11. Hulse, Charles O., and Pask, Joseph A.: Mechanical Properties of Magnesia Single Crystals in Compression. Jour. Am. Ceramic Soc., vol. 43, no. 7, July 1960, pp. 373-378.

12. Fisher, J. C., Johnston, W. G., Thomson, R., and Vreeland, T., Jr., eds.: Dislocations and Mechanical Properties of Crystals. John Wiley & Sons, Inc., 1956.

13. Westwood, A. R. C.: The Surface-Sensitive Mechanical Behavior of Ionic Crystals. Materials Sci. Res., Vol. I, H. H. Stadelmaier and W. W. Austin, eds., 1963, p. 114.

14. Nadeau, John S.: Radiation Hardening in Alkali-Halide Crystals. Jour. Appl. Phys., vol. 34, no. 4, Apr. 1964, pp. 1248-1255.

"The aeronautical and space activities of the United States shall be conducted so as to contribute . . . to the expansion of human knowledge of phenomena in the atmosphere and space. The Administration shall provide for the widest practicable and appropriate dissemination of information concerning its activities and the results thereof."

—NATIONAL AERONAUTICS AND SPACE ACT OF 1958

NASA SCIENTIFIC AND TECHNICAL PUBLICATIONS

TECHNICAL REPORTS: Scientific and technical information considered important, complete, and a lasting contribution to existing knowledge.

TECHNICAL NOTES: Information less broad in scope but nevertheless of importance as a contribution to existing knowledge.

TECHNICAL MEMORANDUMS: Information receiving limited distribution because of preliminary data, security classification, or other reasons.

CONTRACTOR REPORTS: Technical information generated in connection with a NASA contract or grant and released under NASA auspices.

TECHNICAL TRANSLATIONS: Information published in a foreign language considered to merit NASA distribution in English.

TECHNICAL REPRINTS: Information derived from NASA activities and initially published in the form of journal articles.

SPECIAL PUBLICATIONS: Information derived from or of value to NASA activities but not necessarily reporting the results of individual NASA-programmed scientific efforts. Publications include conference proceedings, monographs, data compilations, handbooks, sourcebooks, and special bibliographies.

Details on the availability of these publications may be obtained from:

SCIENTIFIC AND TECHNICAL INFORMATION DIVISION

NATIONAL AERONAUTICS AND SPACE ADMINISTRATION

Washington, D.C. 20546